Single-Element Heterovalent Doping Strategy Stabilizing the Cathode Structure for Reversible Zinc-Ion Storage to Power Soft Robotics

Yameng Zhu[a, b], Xiaona Wang [b, c**], Jiajia Xia[b], Xuechun Wang [b], Ying Kong [b], Yurong Zhou[d], Shuxuan Qu,[b] Wei Feng[a*], Jiangtao Di [b**]

a College of Chemistry, Chemical Engineering and Resource Utilization, Northeast Forestry University, Harbin 150040, China
b Jiangsu Key Laboratory of Organoid Engineering and Precision Medicine, Advanced Materials Division, Suzhou Institute of Nano-Tech and Nano-Bionics, Chinese Academy of Sciences, Suzhou 215123, China
c Guangdong Institute of Semiconductor Micro-Nano Manufacturing Technology, Foshan 528216, China
d International Iberian Nanotechnology Laboratory (INL), Braga 4715330, Portuga

Corresponding E-mail:
wfeng@nefu.edu.cn
xnwang2016@sinano.ac.cn
jtdi2009@sinano.ac.cn
* College of Chemistry, Chemical Engineering and Resource Utilization, Northeast Forestry University, Harbin 150040, China
** Jiangsu Key Laboratory of Organoid Engineering and Precision Medicine, Key Laboratory of Multifunctional Nanomaterials and Smart Systems, Advanced Materials Division, Suzhou Institute of Nano-Tech and Nano-Bionics, Chinese Academy of Sciences, Suzhou 215123, China

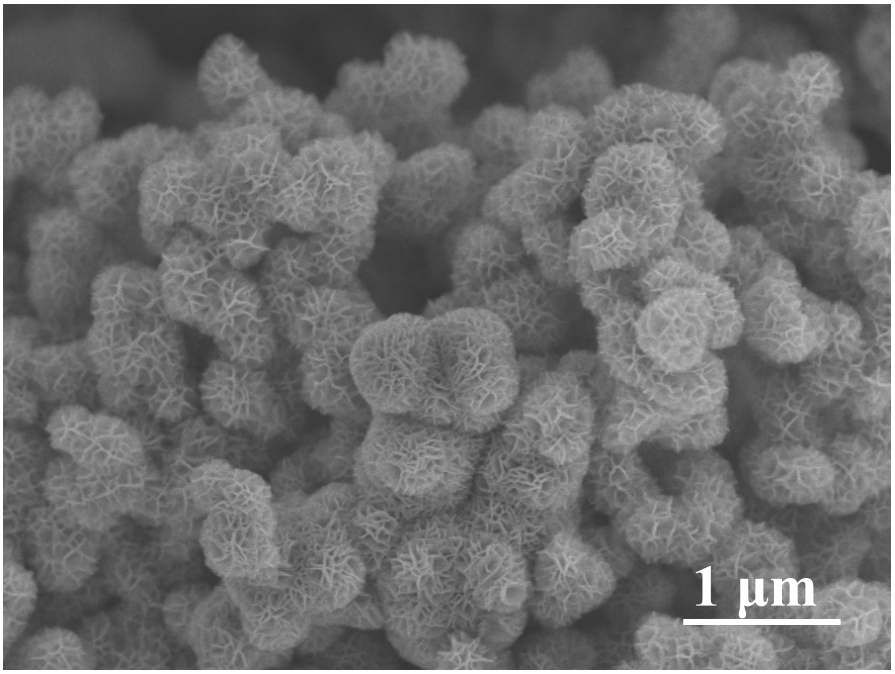

Figure S1 SEM image of δ-MnO_2

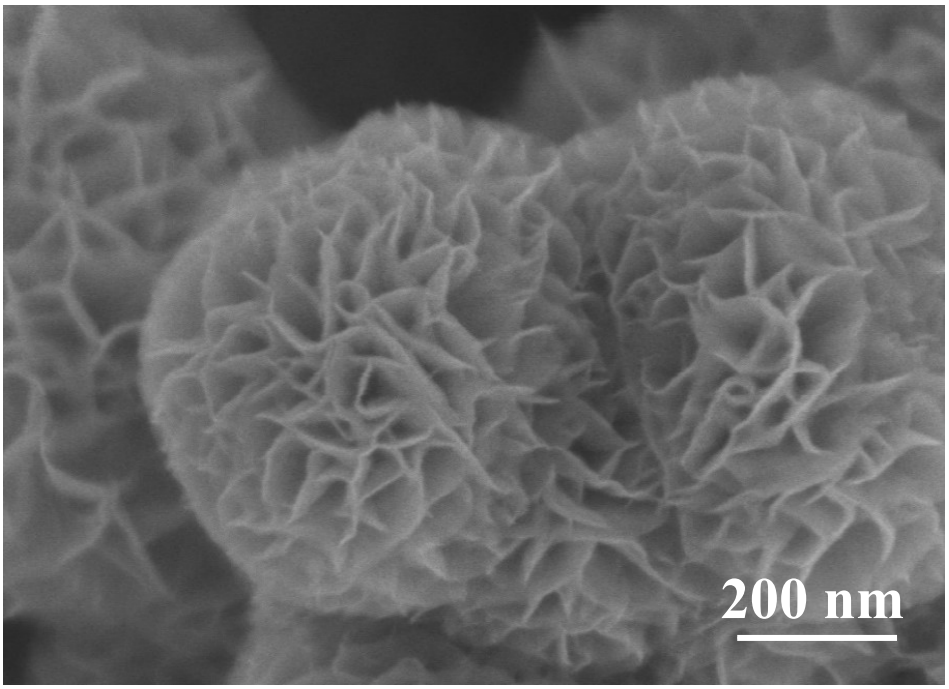

Figure S2 SEM image of δ-MnO_2

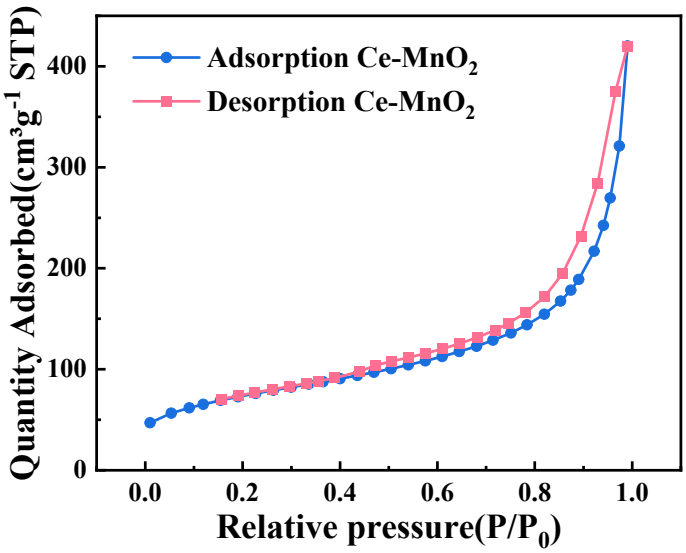

Figure S3 Nitrogen adsorption and desorption isotherms of Ce-MnO_2

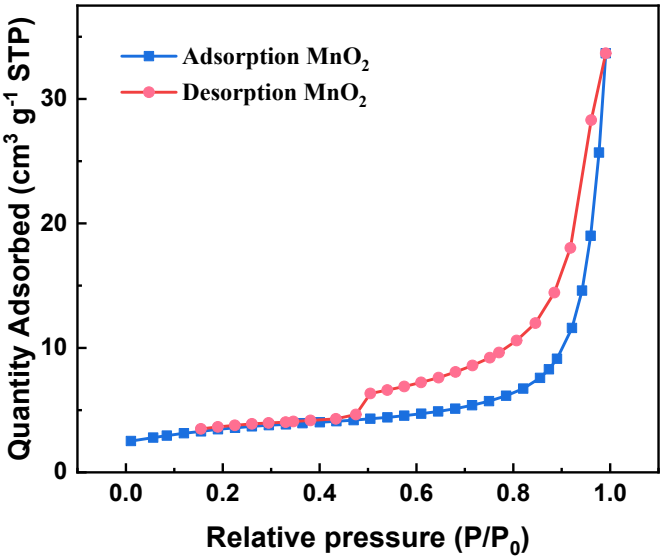

Figure S4 Nitrogen adsorption and desorption isotherms of δ-MnO_2

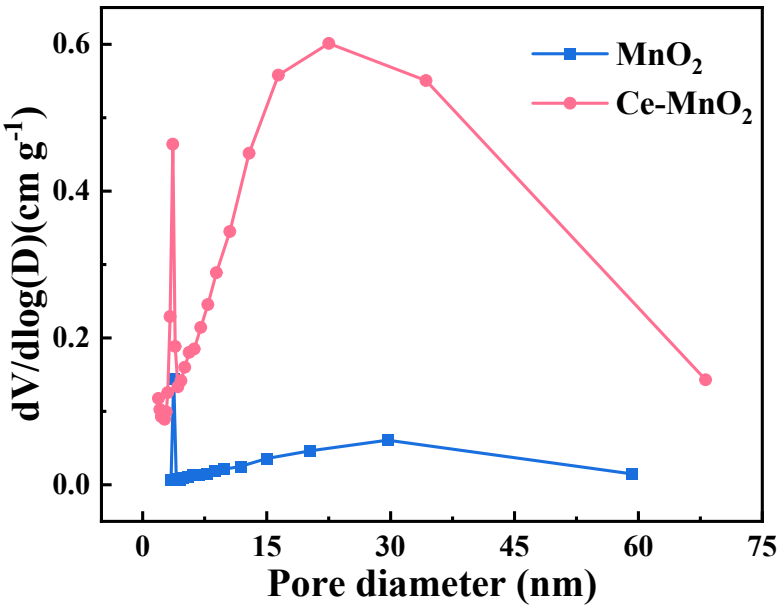

Figure S5 Pore size distribution of Ce-MnO_2 and δ-MnO_2

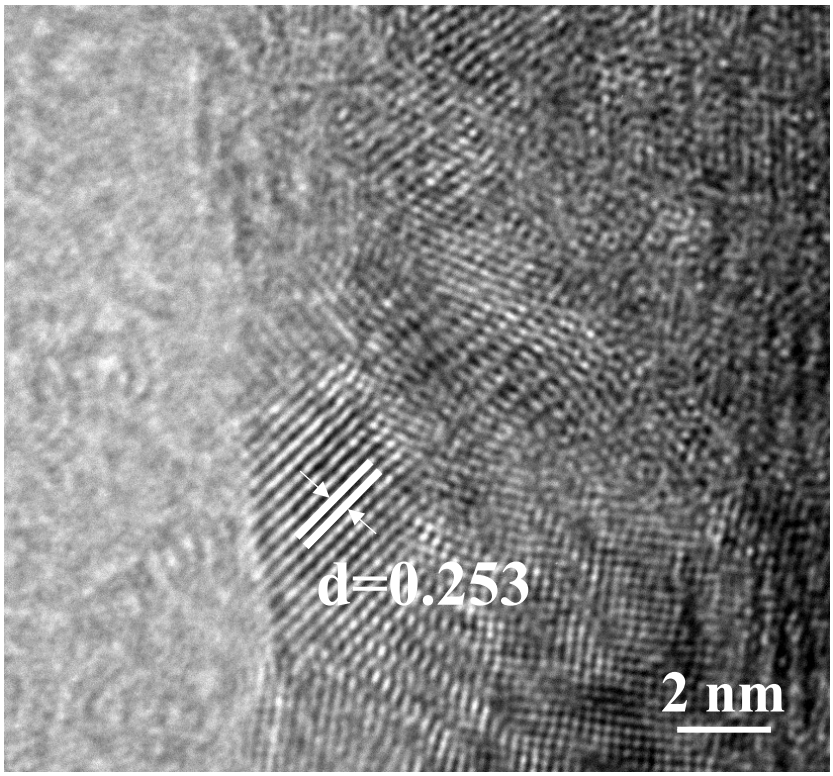

Figure S6 HRTEM image of δ-MnO_2

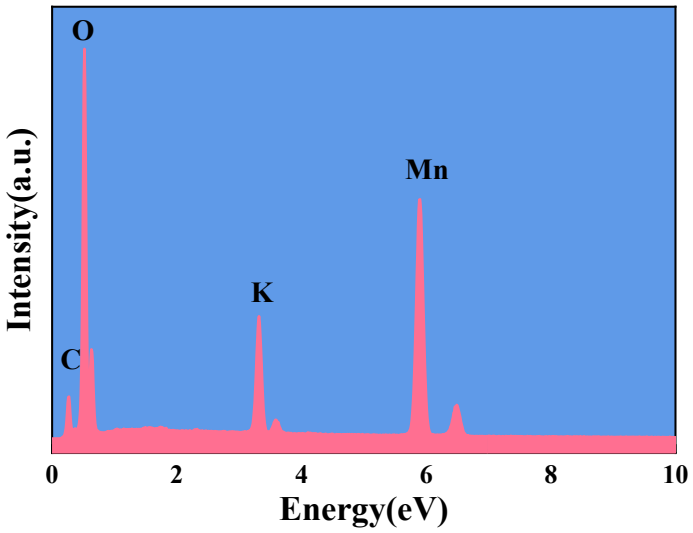

Figure S7 Corresponding EDX element mapping of δ-MnO_2

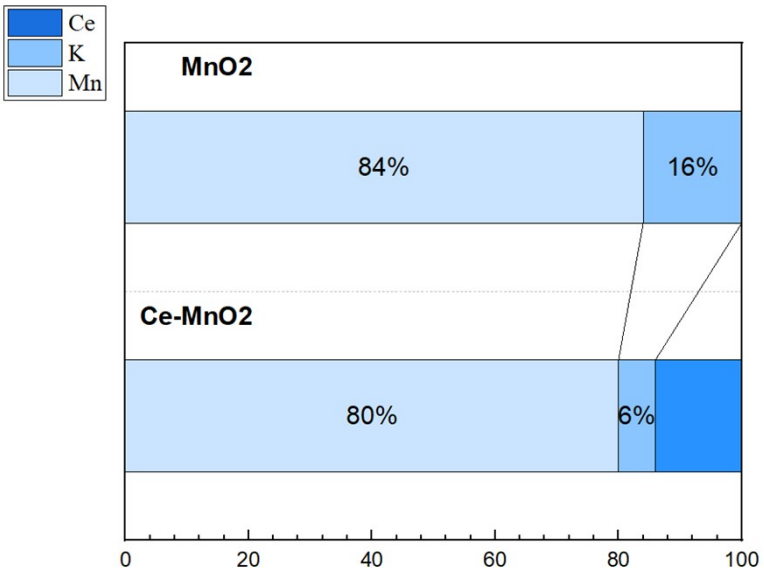

Figure S8 The contents of Mn, K, and Ce elements

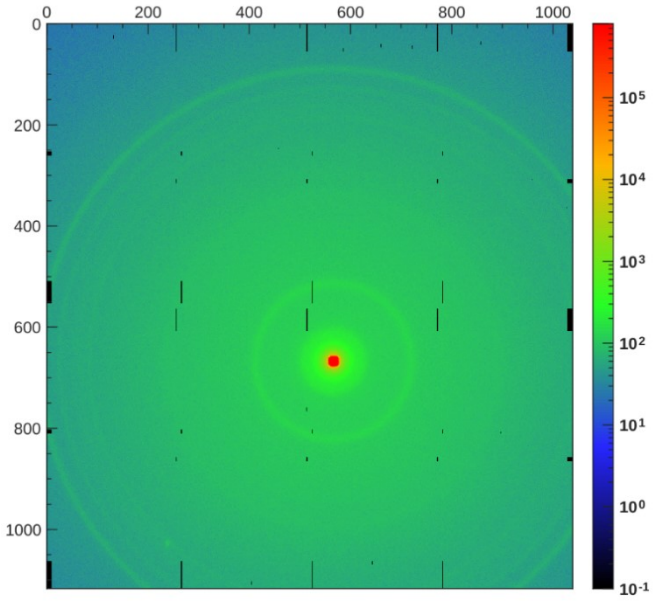

Figure S9 2D WAXS image of δ-MnO_2

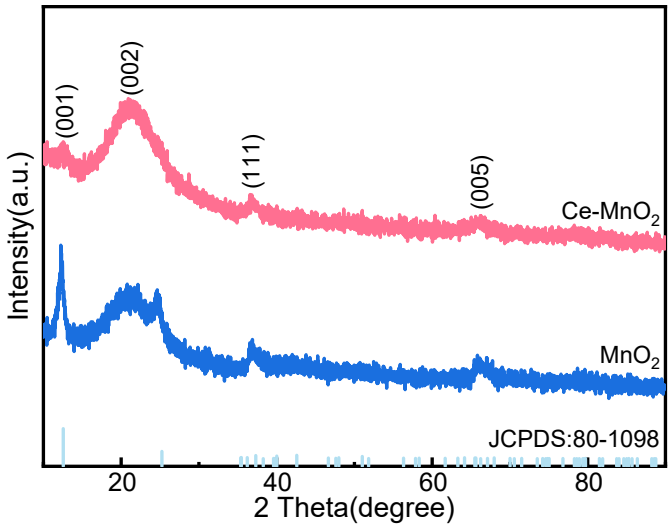

Figure S10 XRD image of δ-MnO_2 and Ce-MnO_2

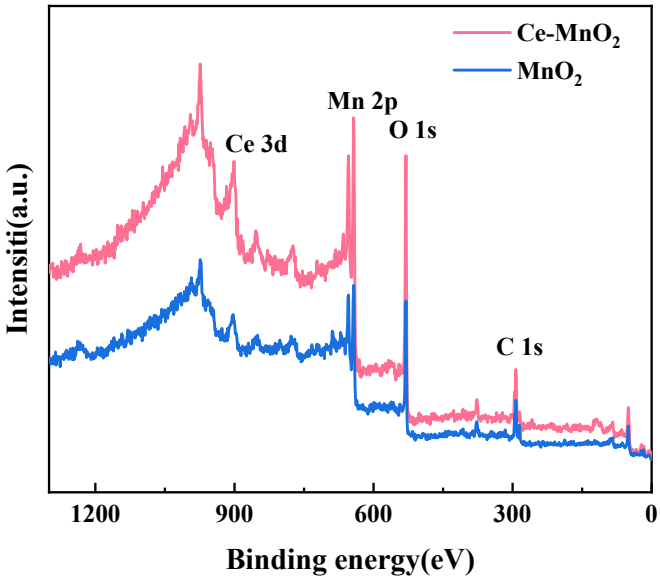

Figure S11 High-resolution XPS spectra of δ-MnO_2 and Ce-MnO_2

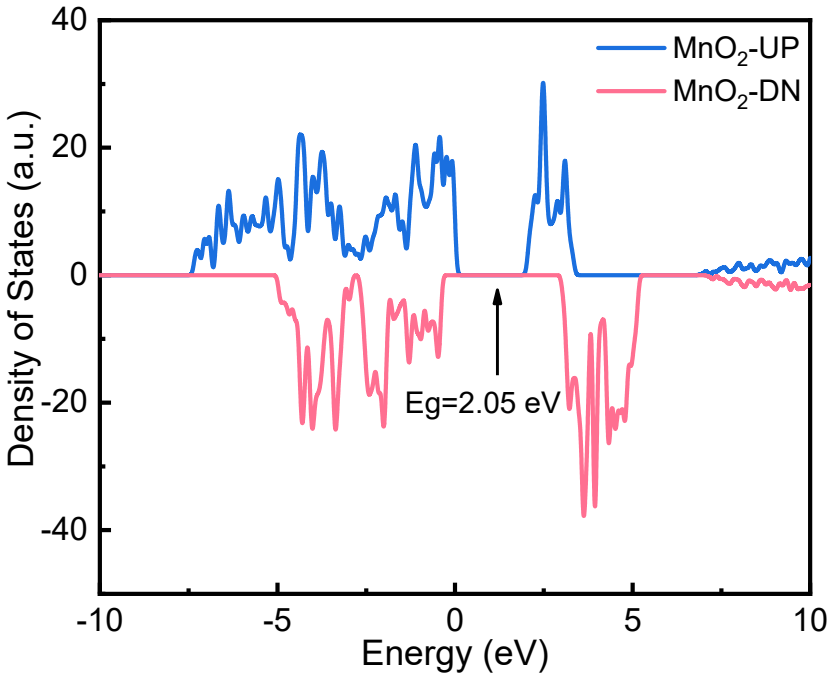

Figure S12 The density of δ-MnO_2 accompanied with oxygen vacancy

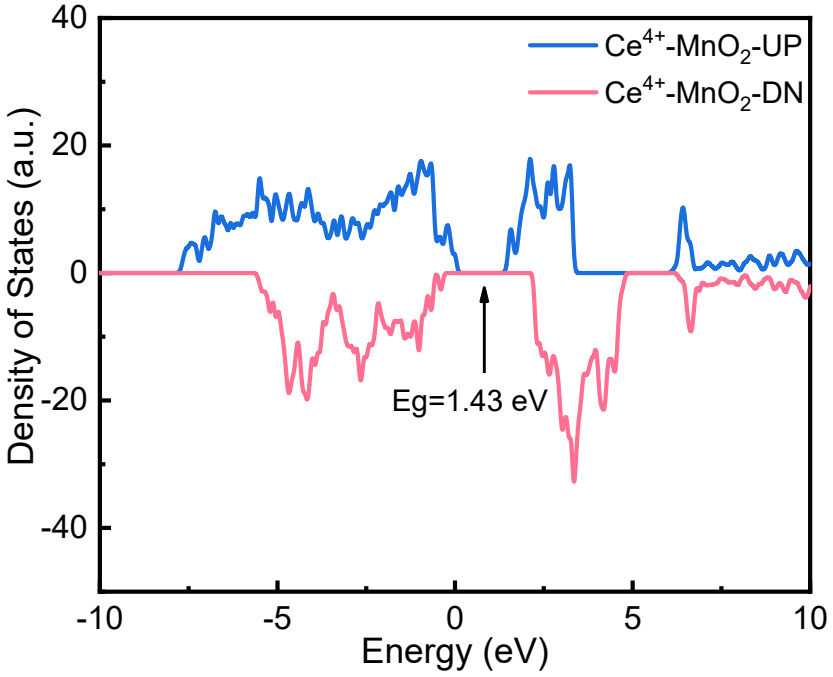

Figure S13 The density of Ce^{4+} doped into δ-MnO_2 accompanied with oxygen vacancy

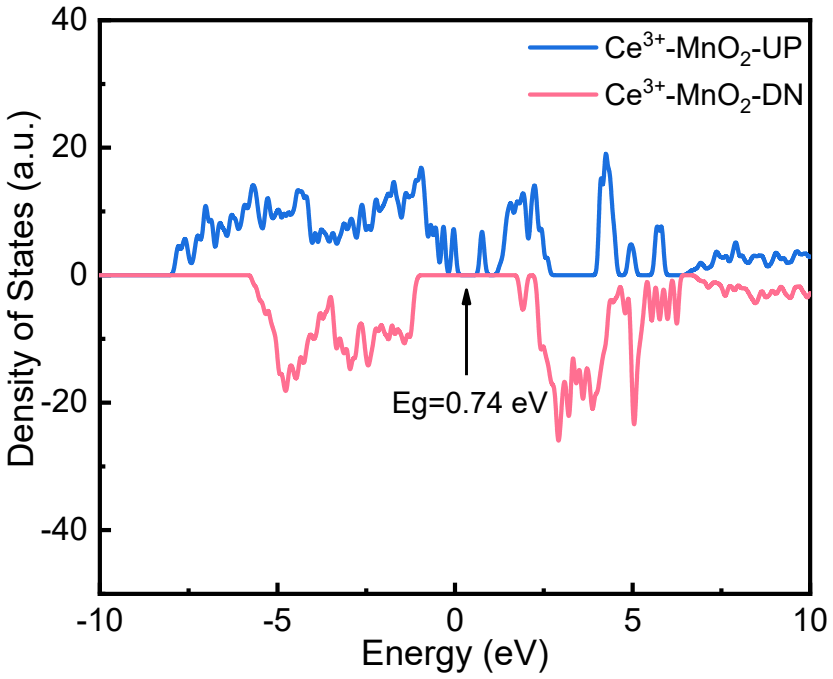

Figure S14 The density of Ce^{3+} doped into δ-MnO_2 accompanied with oxygen vacancy

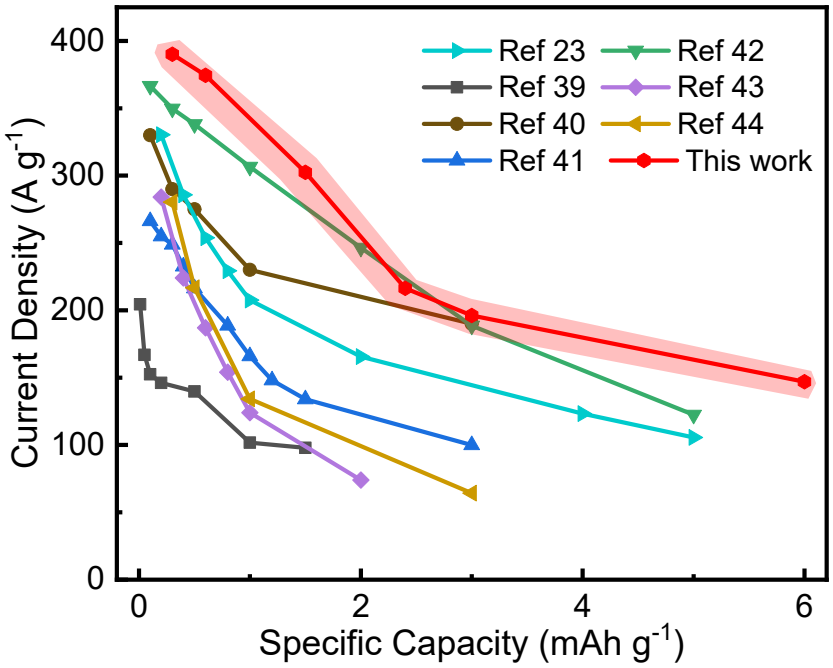

Figure S15 Comparison of rate performance of Ce-MnO_2 with recently reported heteroatom doping of MnO_2 for AZIBs

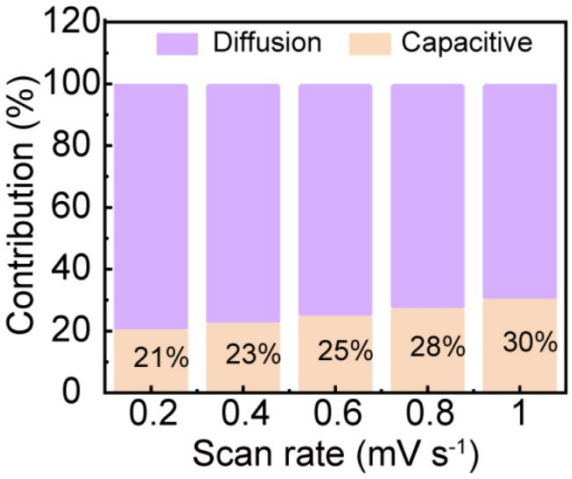

Figure S16 Contribution ratios of the capacitive capacities and diffusion-controlled capacities of the δ-MnO_2 electrode

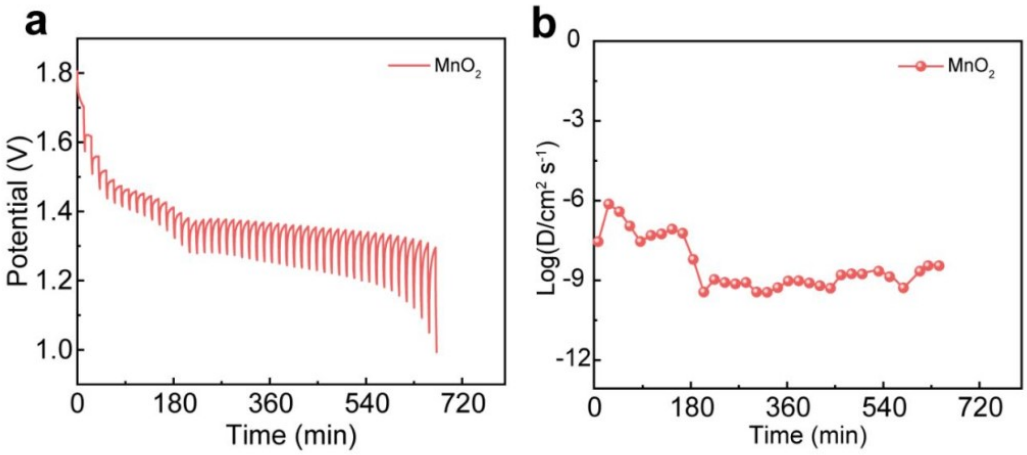

Figure S17 a) Discharging GITT curves at a current density of 0.3 A g^{-1}.
b) Ions diffusion coefficient of δ-MnO_2 during the discharging process

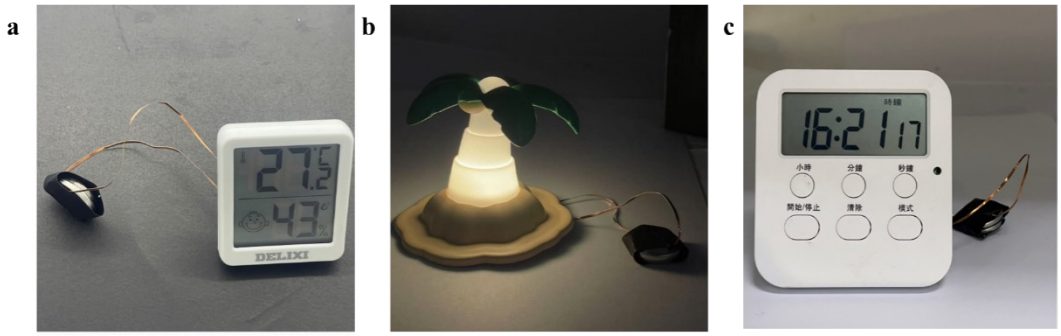

Figure S18 a) The temperature and humidity display, b) the light bulb and c) the clock test by Ce-MnO_2 batteries.